Organic & Biomolecular Chemistry

PAPER

View Article Online
View Journal | View Issue

Cite this: *Org. Biomol. Chem.*, 2017, **15**, 6613

Improved i-motif thermal stability by insertion of anthraquinone monomers†

Alaa S. Gouda,[a,b] Mahasen S. Amine[b] and Erik B. Pedersen *[a]

Received 8th June 2017,
Accepted 20th July 2017

DOI: 10.1039/c7ob01393k

rsc.li/obc

In order to gain insight into how to improve thermal stability of i-motifs when used in the context of biomedical and nanotechnological applications, novel anthraquinone-modified i-motifs were synthesized by insertion of 1,8-, 1,4-, 1,5- and 2,6-disubstituted anthraquinone monomers into the **TAA** loops of a 22mer cytosine-rich human telomeric DNA sequence. The influence of the four anthraquinone linkers on the i-motif thermal stability was investigated at 295 nm and pH 5.5. Anthraquinone monomers modulate the i-motif stability in a position-depending manner and the modulation also depends on the substitution pattern of the anthraquinone. The insertion of anthraquinone was found to stabilize the i-motif structure when replacing any one of the positions of the central **TAA** loop and the thermal stabilities were typically higher than those previously found for i-motifs containing pyrene-modified uracilyl unlocked nucleic acid monomers or twisted intercalating nucleic acid. The 2,6-disubstituted anthraquinone linker replacing $\mathbf{T_{10}}$ enabled a significant increase of i-motif thermal melting by 8.2 °C. A substantial increase of 5.0 °C in i-motif thermal melting was recorded when both $\mathbf{A_6}$ and $\mathbf{T_{16}}$ were modified with a double replacement by the 2,6-isomer into the **TAA** loops in the outer regions. The largest destabilization is observed for the 1,5-disubstituted anthraquinone linker upon the replacement of $\mathbf{A_{18}}$. CD curves of anthraquinone-modified variants imply no structural changes in all cases under potassium buffer conditions compared with those of the native i-motif. Molecular modeling studies explained the increased thermal stabilities of anthraquinone-modified i-motifs.

Introduction

A large body of data obtained during the past 20 years shows that DNA is able to assume alternative and non-canonical structures, in particular within sequences rich in cytosine.[1,2] C-Rich strands with the potential to induce i-motif structures appear repeatedly in the human genome, and several proteins can bind selectively with the C-rich strands.[3,4] i-Motif DNA is found not only in natural sequences of telomeric ends, centromers, introns, and satellite DNA,[5–7] but also in the insulin-linked polymorphic region.[8] A potential role of the i-motif structure in transcriptional regulation has been proposed only recently.[9–11]

In contrast to Watson and Crick duplex, i-motifs are four-stranded intercalated structures of nucleic acids formed by the association of two parallel, right-handed DNA stranded duplexes under acidic pHs (4–6) connected by hemi-protonated cytosine$^+$–cytosine base pairs intercalating with each other by head-to-tail interactions[2,12–14] (Fig. 1). The two duplexes are intercalated in opposite orientations. The i-Motif DNA structures are characterized by different intercalation and folding topologies depending on the DNA sequence.[5] Unlike the G-quadruplexes found in promoters that are stable under physiological conditions in single-stranded templates, i-motifs are far more dynamic and more stable in acidic media, because i-motif formation requires the protonation of one of the cytosines of each base pair.[15] Since 2003, this property has been exploited in the design of hundreds of pH-driven nanomachines.[16] i-Motifs can also exist at neutral pH under molecular crowded conditions[17] and under transcriptionally induced negative superhelicity.[10] Interestingly, DNA, but not RNA, can form i-motifs because in DNA there is a close contact between the deoxyribose sugars in the narrow groove that can give rise to favorable van der Waals interactions.[18] Under negative supercoiling conditions, i-motifs can be formed from duplex DNA and occur even in the absence of a G-quadruplex on the opposite strand.[10]

[a]*Department of Physics, Chemistry and Pharmacy, University of Southern Denmark, Campusvej 55, 5230 Odense M, Denmark. E-mail: Erik@sdu.dk; Fax: +45 66158780*
[b]*Department of Chemistry, Faculty of Science, Benha University, Benha, 13518, Egypt*

†Electronic supplementary information (ESI) available: CD spectral analysis of 22mer C-rich human telomeric DNA sequence **ON1** and anthraquinone-modified i-motif variants **ON2–ON33** (Fig. S1–S3). Normalized UV absorption melting curves and first derivatives for anthraquinone-modified i-motifs (Fig. S4–S6). Maldi-TOF mass spectrometry data of calculated and found mass (Table S1). Maldi mass spectrometry data of oligonucleotides (**ON1–ON33**). See DOI: 10.1039/c7ob01393k

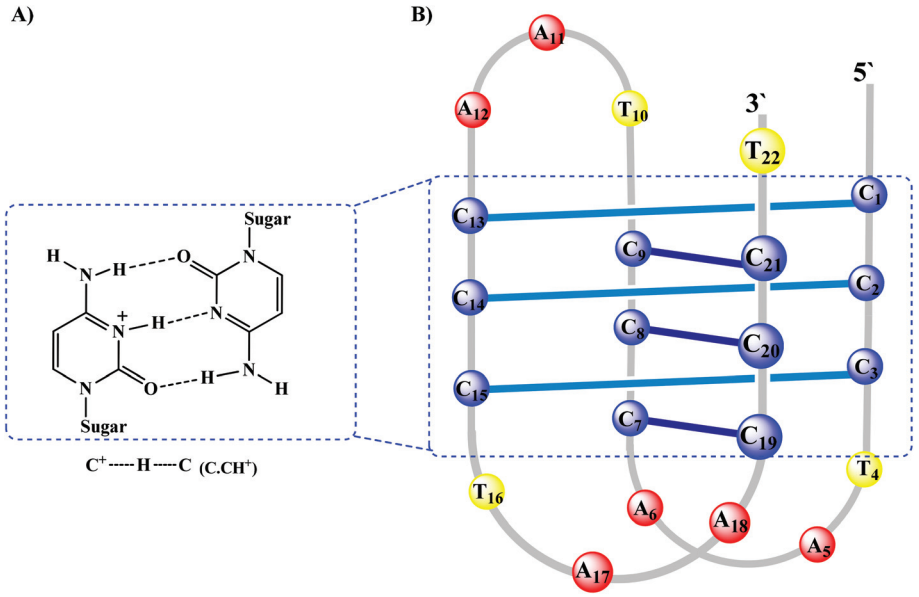

Fig. 1 Folding topology of the human telomeric DNA i-motif: (A) hemiprotonated C^+···H···C base pair, (B) intramolecular structure of human telomeric DNA i-motif 5′-d[$(CCCTAA)_3CCCT$] with a 5′E intercalation topology.

Chemically modified i-motif structures are interesting to study because i-motifs have attracted a great deal of interest for their implication in biological processes[5–7,19,20] and are considered important for the progress of DNA-nanotechnology,[1] diagnostics and therapeutics[13,21–24] due to their rapid transformations and sensitivity to variations in pH.[25]

In this work, we modify one of the best described i-motif sequences, the 22mer fragment of human telomeric DNA with the sequence 5′-d[$(CCCTAA)_3CCCT$]. This C-rich DNA fragment is a part of the 5′-tail at the telomere end of chromosomes in the S phase of replication and directly correlates with the proliferative rate of human cell cultures.[26–28] In accord with NMR studies, the C-rich human telomeric i-motif folds intramolecularly.[3,29] The core of this i-motif possesses six C–C^+ base pairs with 2′-deoxycytidine placed at the 5′-extremity of each stretch (Fig. 1). Furthermore, the core is linked by a central **TAA** loop bridging a narrow groove and two external **TAA** loops located across the wide grooves.[5] Only a few reports can be found on the modification of the nucleobase in i-motifs.[5,30–33] The major aim of this study is to explore the stability properties upon the replacement of nucleotides in the **TAA** loops of the 22mer i-motif by anthraquinone monomers.

Anthraquinone monomers are known to modulate the stability of duplexes and G-quadruplexes.[34,35] Furthermore, it has been reported that anthraquinone modified G-quadruplexes efficiently downregulate genomic HRAS in bladder cancer cells and inhibit cell growth through a decoy mechanism, wherein the anthraquinone-modified G-quadruplexes mimic the G-quadruplexes located near the major transcriptional start site in the HRAS promoter.[35] The decoy effect is comparable to the previous reported decoy effect of TINA quadruplexes toward oncogenic HRAS genes for cancer therapy.[36] In addition, anthraquinone monomers were potent modulators of G-quadruplex thermodynamic stability being able to change the binding affinity and biological properties of a quadruplex-based thrombin binding aptamer (TBA) and to improve its potency to inhibit fibrin-clot formation.[37] Not surprisingly, mitoxantrone, an anthraquinone analogue, has recently been found to both bind and stabilize i-motif forming DNA sequences at neutral pH preferentially over double helical DNA.[38] Furthermore, the low reduction potential of anthraquinones opens possibilities for charge transport in i-motif DNA.[39]

Herein, anthraquinone-modified i-motifs were synthesized using the phosphoramidite chemistry approach. They were modified at positions in the central and the external **TAA** loops by anthraquinone monomers $\mathbf{H_{18}}$, $\mathbf{H_{14}}$, $\mathbf{H_{15}}$ and $\mathbf{H_{26}}$ (Fig. 2) synthesized previously by our research group.[37,40] To the best of our knowledge this is the first report describing the incorporation of dipropoxylated anthraquinones into i-motif DNA.

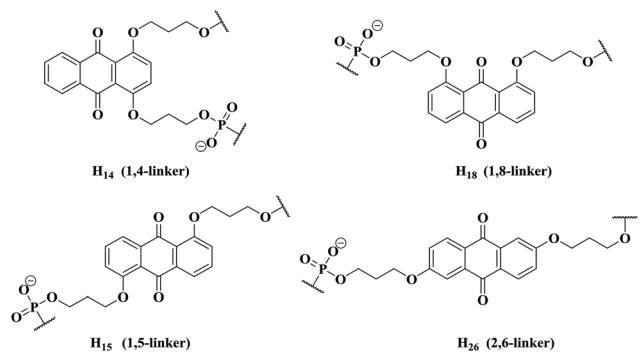

Fig. 2 The 1,4-, 1,8-, 1,5- and 2,6-disubstituted anthraquinone building blocks (H_{14}, H_{18}, H_{15} and H_{26}).

Results and discussion

Thermal stability and circular dichroism of anthraquinone i-motifs

The influence of the aforementioned four non-nucleosidic building blocks on the thermal stability of i-motif was evaluated by thermal denaturation experiments using the UV absorption melting method at 295 nm and pH 5.5. As depicted in Table 1, we first replaced the three nucleotides in the central **TAA** ($\mathbf{T_{10}}$, $\mathbf{A_{11}}$, and $\mathbf{A_{12}}$) loop of the parental oligonucleotide **ON1** one by one with the four anthraquinone linkers $\mathbf{H_{18}}$, $\mathbf{H_{14}}$, $\mathbf{H_{15}}$ and $\mathbf{H_{26}}$ resulting in twelve different anthraquinone modified variants **ON2–ON13**. Actually, all anthraquinone modifications of the central **TAA** loop resulted in more stabilized i-motifs. For all possible replacements of one nucleotide with $\mathbf{H_{14}}$, $\mathbf{H_{18}}$, $\mathbf{H_{15}}$ or $\mathbf{H_{26}}$, the thermal melting (T_m °C) increased in the range 1.1 to 8.2 °C. The minimum improvement in T_m was found with the replacement of $\mathbf{T_{10}}$ with $\mathbf{H_{18}}$, whereas the replacement of $\mathbf{T_{10}}$ with $\mathbf{H_{26}}$ revealed the maximum increase in T_m. In fact, only a small increase in T_m ranging from 1.1 to 1.4 °C was observed for the replacement with $\mathbf{H_{18}}$ (**ON2–ON4**), whereas the increase in T_m from 2.0 to 3.4 °C was slightly larger for the corresponding replacement with $\mathbf{H_{14}}$ (**ON5–ON7**), the largest one being an increase of 3.4 °C for the replacement of $\mathbf{A_{11}}$ (**ON6**). The increase in T_m from 2.0 to 4.0 °C for $\mathbf{H_{15}}$ is comparable with the increase for $\mathbf{H_{14}}$, but the thermal stabilities of the $\mathbf{H_{15}}$ modified i-motifs **ON8–ON10** increase in the order $\mathbf{A_{12}} < \mathbf{A_{11}} < \mathbf{T_{10}}$ which differs from the order $\mathbf{A_{12}} < \mathbf{T_{10}} < \mathbf{A_{11}}$ for $\mathbf{H_{14}}$ modified i-motifs. This behavior could be compatible with previously reported data showing that $\mathbf{T_{10}}$ in the unmodified i-motif DNA stacks on the i-motif core as a hydrogen-bonded base pair with $\mathbf{T_{22}}$, while $\mathbf{A_{11}}$ is situated above being involved in stacking interactions, together with hydrogen bonding with $\mathbf{T_{22}}$ through water molecules.[33,41] Therefore, it is favorable to replace $\mathbf{T_{10}}$ or $\mathbf{A_{11}}$ with the stacking anthraquinone moieties $\mathbf{H_{14}}$ and $\mathbf{H_{15}}$. In contrast, we assume that $\mathbf{A_{12}}$ is positioned outward relative to the i-motif core and its replacement with $\mathbf{H_{14}}$ or $\mathbf{H_{15}}$ is therefore not likely to result in better stacking interactions. Interestingly, the $\mathbf{H_{26}}$ monomer placed in position $\mathbf{T_{10}}$ (**ON11**) causes a significant increase of i-motif thermal stability resulting in a ΔT_m of 8.2 °C. Surprisingly, the increase in the T_m value was higher for the replacement of $\mathbf{A_{12}}$ (**ON13**) with a ΔT_m of 5.4 °C than for $\mathbf{A_{11}}$ (**ON12**) with a ΔT_m of 2.4 °C. It could be of interest to gain more insight into the stabilizing effect of $\mathbf{H_{26}}$ upon the replacement of $\mathbf{T_{10}}$ by studying the stacking modes as indicated by molecular modeling (*vide infra*). The ΔT_m values shown in Table 1 are in agreement with the previous observations that an increased level of flexibility in the loop regions (positions **4**, **10–12** and **16**) is favourable for i-motif stability.[5] In accordance with the aforementioned data, we may conclude that the efficacy of anthraquinone linkers upon replacement in the central **TAA** sequence increased in the order $\mathbf{H_{18}} < \mathbf{H_{14}} \sim \mathbf{H_{15}} < \mathbf{H_{26}}$. It should be noted that anthraquinone monomers have a stabilizing influence on the central **TAA** loop reflecting higher thermal stabilities than those observed for pyrene-modified uracil UNA monomers[32] and for the pyrene intercalator TINA.[33] Anthraquinone monomers also have a better stabilizing effect than UNA(U)[5] when replacing $\mathbf{T_{10}}$ and UNA(A)[5] when replacing $\mathbf{A_{11}}$.

To assert the formation of i-motifs **ON1–ON13**, circular dichroism (CD) spectra were recorded. They all showed the characteristic feature of an i-motif with positive maxima around 285–290 nm and negative minima around 255–260 nm though with lower amplitudes than those of the corresponding wild type i-motif (Fig. S1, ESI†).

Another point of interest is to investigate double replacements at positions in the i-motif where mutual stacking interactions are possible. We selected the replacement of both $\mathbf{A_6}$ and $\mathbf{T_{16}}$ in the unmodified i-motif **ON1** with anthraquinone monomers resulting in four different anthraquinone modified variants **ON14–ON17**. The reason for selecting these positions is based on the structure 1El2 from the Brookhaven Protein Data Bank which revealed that $\mathbf{A_6}$ and $\mathbf{T_{16}}$ are in a stacking mode. However, as shown in Table 2, the incorporation of a pair of 1,8-, 1,4- or 1,5-derivatives in the i-motif **ON14–ON16**

Table 1 T_m and ΔT_m (○C) for the melting of i-motifs evaluated from the UV melting curves (**ON1–ON13**)

Code [°C]	Entry	Sequence	T_m [a] [°C]	ΔT_m [b]
ON1	Wild type	5′-CCC TAA CCC TAA CCC TAA CCC T-3′	41.6	—
ON2	T_{10}	5′-CCC TAA CCC $\mathbf{H_{18}}$AA CCC TAA CCC T-3′	42.7	1.1
ON3	A_{11}	5′-CCC TAA CCC T$\mathbf{H_{18}}$A CCC TAA CCC T-3′	43.0	1.4
ON4	A_{12}	5′-CCC TAA CCC TA$\mathbf{H_{18}}$ CCC TAA CCC T-3′	42.8	1.2
ON5	T_{10}	5′-CCC TAA CCC $\mathbf{H_{14}}$AA CCC TAA CCC T-3′	43.8	2.2
ON6	A_{11}	5′-CCC TAA CCC T$\mathbf{H_{14}}$A CCC TAA CCC T-3′	45.0	3.4
ON7	A_{12}	5′-CCC TAA CCC TA$\mathbf{H_{14}}$ CCC TAA CCC-T-3′	43.6	2.0
ON8	T_{10}	5′-CCC TAA CCC $\mathbf{H_{15}}$AA CCC TAA CCC T-3′	45.6	4.0
ON9	A_{11}	5′-CCC TAA CCC T$\mathbf{H_{15}}$A CCC TAA CCC T-3′	45.0	3.4
ON10	A_{12}	5′-CCC TAA CCC TA$\mathbf{H_{15}}$ CCC TAA CCC T-3′	43.6	2.0
ON11	T_{10}	5′-CCC TAA CCC $\mathbf{H_{26}}$AA CCC TAA CCC T-3′	49.8	8.2
ON12	A_{11}	5′-CCC TAA CCC T$\mathbf{H_{26}}$A CCC TAA CCC T-3′	44.0	2.4
ON13	A_{12}	5′-CCC TAA CCC TA$\mathbf{H_{26}}$ CCC TAA CCC-T-3′	47.0	5.4

[a] 4 μM oligonucleotides at 295 nm in potassium buffer (100 mM KCl + 20 mM K_2HPO_4, pH = 5.5 and 1 mM K_2EDTA). [b] Difference in T_m relative to wild-type **ON1**. Melting temperatures are within the uncertainty of ±0.5 °C as determined by repetitive experiments and the T_m values were calculated taking an average of the two melting curves.

Table 2 T_m and ΔT_m (°C) for the melting of i-motifs evaluated from the UV melting curves (**ON1** and **ON14–ON29**)

Code [°C]	Entry	Sequence	T_m [a] [°C]	ΔT_m [b]
ON1	Wild type	5′-CCC TAA CCC TAA CCC TAA CCC T-3′	41.6	—
ON14	A_6T_{16}	5′-CCC TA**H$_{18}$** CCC TAA CCC **H$_{18}$**AA CCC T-3′	38.6	−3.0
ON15	A_6T_{16}	5′-CCC TA**H$_{14}$** CCC TAA CCC **H$_{14}$**AA CCC T-3′	39.0	−2.6
ON16	A_6T_{16}	5′-CCC TA**H$_{15}$** CCC TAA CCC **H$_{15}$**AA CCC T-3′	37.0	−3.6
ON17	A_6T_{16}	5′-CCC TA**H$_{26}$** CCC TAA CCC **H$_{26}$**AA CCC T-3′	46.6	5.0
ON18	A_6T_{16}	5′-CCC TA**H$_{18}$** CCC TAA CCC **H$_{14}$**AA CCC T-3′	36.8	−4.8
ON19	A_6T_{16}	5′-CCC TA**H$_{18}$** CCC TAA CCC **H$_{15}$**AA CCC T-3′	39.0	−2.6
ON20	A_6T_{16}	5′-CCC TA**H$_{18}$** CCC TAA CCC **H$_{26}$**AA CCC T-3′	42.8	1.2
ON21	A_6T_{16}	5′-CCC TA**H$_{14}$** CCC TAA CCC **H$_{18}$**AA CCC T-3′	39.6	−2.0
ON22	A_6T_{16}	5′-CCC TA**H$_{14}$** CCC TAA CCC **H$_{15}$**AA CCC T-3′	38.2	−3.4
ON23	A_6T_{16}	5′-CCC TA**H$_{14}$** CCC TAA CCC **H$_{26}$**AA CCC T-3′	40.8	−0.8
ON24	A_6T_{16}	5′-CCC TA**H$_{15}$** CCC TAA CCC **H$_{18}$**AA CCC T-3′	38.4	−3.2
ON25	A_6T_{16}	5′-CCC TA**H$_{15}$** CCC TAA CCC **H$_{14}$**AA CCC T-3′	37.6	−4.0
ON26	A_6T_{16}	5′-CCC TA**H$_{15}$** CCC TAA CCC **H$_{26}$**AA CCC T-3′	40.6	−1.0
ON27	A_6T_{16}	5′-CCC TA**H$_{26}$** CCC TAA CCC **H$_{18}$**AA CCC T-3′	42.6	1.0
ON28	A_6T_{16}	5′-CCC TA**H$_{26}$** CCC TAA CCC **H$_{14}$**AA CCC T-3′	42.6	1.0
ON29	A_6T_{16}	5′-CCC TA**H$_{26}$** CCC TAA CCC **H$_{15}$**AA CCC T-3′	42.0	0.6

[a] 4 μM oligonucleotides at 295 nm in potassium buffer (100 mM KCl + 20 mM K_2HPO_4, pH = 5.5 and 1 mM K_2EDTA). [b] Difference in T_m relative to wild-type **ON1**. Melting temperatures are within the uncertainty of ±0.5 °C as determined by repetitive experiments and the T_m values were calculated taking an average of the two melting curves.

results in a considerable decrease in T_m. All three regioisomeric modifications reduce the T_m values between −3.6 and −2.6 °C when compared to those of wild-type **ON1**. Only the incorporation of the 2,6-isomer at the same positions leads to an increase in thermostability (ΔT_m = 5.0 °C, **ON17**). We hypothesized that the increased stability of the i-motifs containing one double-inserted anthraquinone monomer **H$_{26}$** (**ON17**) instead of **A$_6$** and **T$_{16}$** is presumably due to improved stacking as indicated by molecular modelling (*vide infra*). Thus, we found that the thermal stabilities of double anthraquinone modified i-motifs increase in the order **H$_{15}$** < **H$_{18}$** < **H$_{14}$** < **H$_{26}$** upon the replacement of **A$_6$** and **T$_{16}$**.

Looking for even better mutual stacking interactions between a pair of anthraquinones, we subsequently studied the effect of mixed pairs placed in **A$_6$** and **T$_{16}$**. All possible mixed pairs were investigated as can be seen in Table 2 for **ON18–ON29**. However, upon the replacement of **A$_6$** and **T$_{16}$** with mixed pairs of **H$_{14}$**, **H$_{18}$** and **H$_{15}$**, a decrease in the T_m values in the range −2.6 °C to −4.8 °C (**ON18**, **ON19**, **ON21**, **ON22**, **ON24** and **ON25**) relative to the wild type **ON1** was observed. For all pairs containing **H$_{26}$** instead of **A$_6$**, a slight increase in T_m around 1.0 °C relative to the unmodified i-motif **ON1** was observed (**ON27–ON29**), whereas the ΔT_m values moved into the range of −1.0 °C to 1.2 °C in mixed pairs containing **H$_{26}$** instead of **T$_{16}$** (ΔT_m = 1.2 °C, **ON20**; −0.8 °C, **ON23**; −1.0 °C, **ON26**). The latter results may reflect the above results for the identical anthraquinone pairs which revealed a 5.0 °C increase in the T_m in the case of **H$_{26}$** (**ON17**). We hence conclude that there is a stabilizing effect of **H$_{26}$** and a destabilizing effect of **H$_{14}$**, **H$_{18}$** and **H$_{15}$** when replacing **A$_6$** and **T$_{16}$** in the i-motif.

The CD spectra of all modified variants **ON14–ON29** show the characteristic profile of an i-motif with intense positive and negative ellipticity at 283–290 nm and 254–260 nm, respectively.[42] The intensity of the bands is not significantly changed relative to those of the unmodified i-motif which suggests that the anthraquinone monomers do not induce any changes in the overall i-motif structure (Fig. S2, ESI†).

To confirm the stabilizing effect of **H$_{26}$** and the destabilizing effect of **H$_{18}$**, **H$_{14}$** and **H$_{15}$** anthraquinone monomers, they were incorporated into position 18 in the outer loop region in the C-rich 22mer fragment of the human telomeric DNA (**ON30–ON33**). As outlined in Table 3, all monomers, except **H$_{26}$**, were found to destabilize the i-motifs in the range −5.0 °C to −7.8 °C with reference to **ON1**, whereas the T_m increased only 0.4 °C for the **H$_{26}$** monomer (**ON33**). The decreased stability of these i-motif structures (**ON30–ON32**) is presumably due to the loss of stacking interactions with nucleobases in the loop region due to structural perturbations. In comparison with the previously reported data,[5] we thus observed that the **H$_{26}$** monomer placed in position **A$_{18}$** has a slightly higher melting temperature than that for UNA(A) at the same position.

Also in this case, the CD spectra of **ON30–ON33** explicated positive amplitudes at 287–292 nm and negative ones at 260–265 nm, although with lower amplitudes than those of the corresponding wild type i-motif. Such data are consistent with the characteristic feature of an i-motif (Fig. S3, ESI†).

From the aforementioned results, we can conclude that the improved stabilities of i-motifs when replacing the nucleotides with the **H$_{26}$** monomer in the loop regions make this anthraquinone monomer a new member of the small group of modifiers stabilizing i-motif structures such as PNA,[43–45] LNA,[13] acyclic UNA,[5] 3′-*S*-phosphorothiolates[46,47] or 2′-deoxy-2′-fluorocytidine.[48]

Molecular modeling

Because increased thermal stabilities of an i-motif containing one single-incorporated monomer **H$_{26}$** (**ON11**) as well as another double-incorporated monomer **H$_{26}$** (**ON17**) were observed leading to ΔT_m of 8.2 °C and 5.0 °C respectively, we decided to evaluate the possibility of **H$_{26}$** involvement in stack-

Table 3 T_m (○C) and ΔT_m (○C) for the melting of i-motifs evaluated from the UV melting curves (**ON1** and **ON30–ON33**)

Code [°C]	Entry	Sequence	T_m [a] [°C]	ΔT_m [b]
ON1	Wild type	5′-CCC TAA CCC TAA CCC TAA CCC T-3′	41.6	—
ON30	A_{18}	5′-CCC TAA CCC TAA CCC TA**H**$_{18}$ CCC T-3′	36.6	−5.0
ON31	A_{18}	5′-CCC TAA CCC TAA CCC TA**H**$_{14}$ CCC T-3′	36.2	−5.4
ON32	A_{18}	5′-CCC TAA CCC TAA CCC TA**H**$_{15}$ CCC T-3′	33.8	−7.8
ON33	A_{18}	5′-CCC TAA CCC TAA CCC TA**H**$_{26}$ CCC T-3′	42.0	0.4

[a] 4 μM oligonucleotides at 295 nm in potassium buffer (100 mM KCl + 20 mM K_2HPO_4, pH = 5.5 and 1 mM K_2EDTA). [b] Difference in T_m relative to wild-type **ON1**. Melting temperatures are within the uncertainty of ±0.5 °C as determined by repetitive experiments and the T_m values were calculated taking an average of the two melting curves.

ing interactions in an i-motif. Upon the replacement of $\mathbf{T_{10}}$ in **ON11**, the i-motif structure thus obtained is depicted in Fig. 3 after performing molecular modeling. A modified AMBER* force field in Macro Model 9.2 molecular modeling was utilized to generate representative low-energy structures of the modified 22mer C-rich sequence. The starting structure of the 22mer C-rich i-motif was downloaded using the Protein Data Bank (PDB) code 1El2 accession number and modified with the anthraquinone monomer $\mathbf{H_{26}}$. The modeling gave us some understanding of the 8.2 °C increase in T_m. The model showed that it was possible for the $\mathbf{H_{26}}$ linker to form a hydrogen bond with cytosine $\mathbf{C_1}$ located in the flanking 5′ end. Furthermore, stacking is observed between $\mathbf{H_{26}}$ and the cytosine base pair $\mathbf{C_1}$–$\mathbf{C_{13}}^+$ as can be seen Fig. 3A. This base pair is already stacked over the other five hemiprotonated cytidine base pairs (Fig. 3B). Another reason for the thermal stability of $\mathbf{H_{26}}$ is believed to be the release of strain in the loop part of the i-motif when compared to the wild type **ON1**.

However, in the case of replacement of both $\mathbf{A_6}$ and $\mathbf{T_{16}}$ with $\mathbf{H_{26}}$, the structural conformation of the two anthraquinone building blocks is completely changed. In other words, the two anthraquinone units are not stacked at all with the cytidine base pairs (Fig. 4A), but the two moieties are stacked on each other in at least one benzene ring in each linker as depicted in Fig. 4B. This could be the reason for the +5 °C increase in T_m in the case of double insertion using $\mathbf{H_{26}}$.

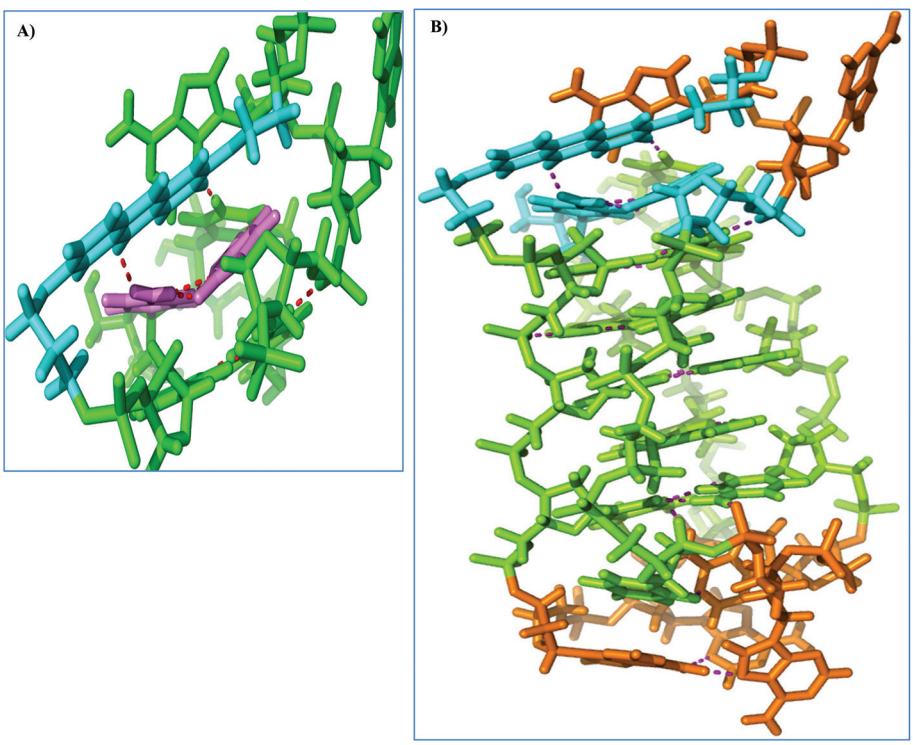

Fig. 3 Representative low-energy structures of an i-motif containing a 2,6-anthraquinone linker (H_{26}) upon the replacement of T_{10} (**ON11**) by an Amber-minimized model: (A) side view displaying hybridization and staking mode interaction between H_{26} linker and cytidine C_1–C_{13}^+ base pair. H_{26} monomer is shown in cyan and cytidines (C_1, C_{13}) are shown in magenta. Hydrogen bonds are displayed in red. The rest of the i-motif strand is marked in green; (B) overall view displaying stacking interactions and overlapping for the possible conformation of **ON11**. H_{26} monomer and cytidine C_1–C_{13}^+ base pair are shown in cyan. Thymidines (T) and adenosines (A) are shown in orange. The other cytidine base pairs are marked in limegreen. Hydrogen bonds are displayed in violet.

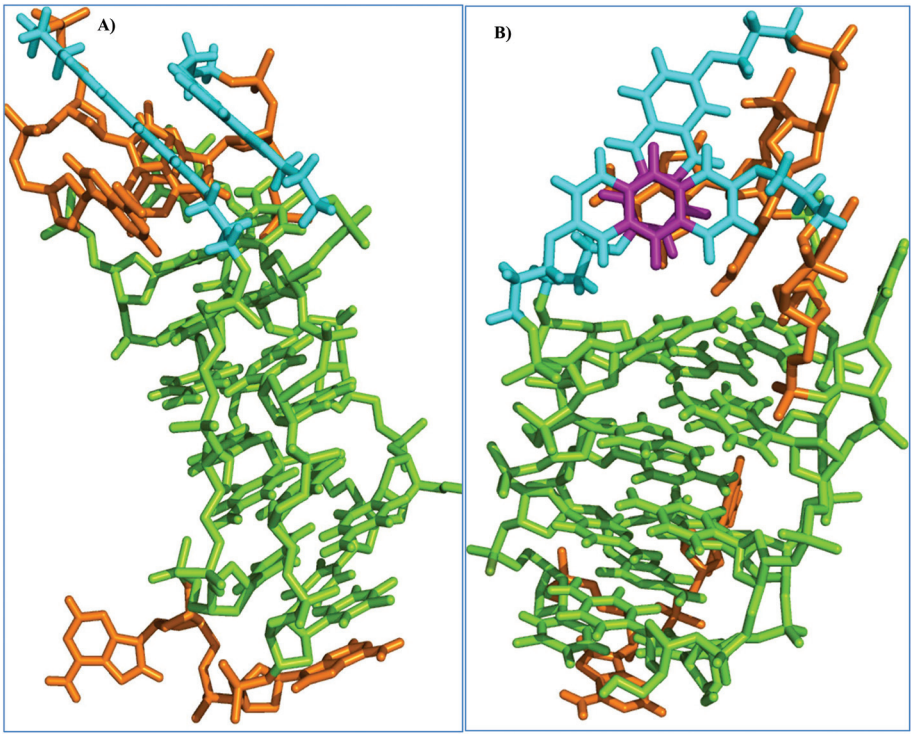

Fig. 4 Representative low-energy structures of an i-motif containing a 2,6-anthraquinone linker (H_{26}) upon the replacement of both A_6 and T_{16} (**ON17**) by an Amber-minimized model: (A) overall view of a possible conformation of **ON17**. H_{26} monomers are shown in cyan and cytidine base pairs are shown in limegreen. Thymidines (**T**) and adenosines (**A**) are shown in orange; (B) front layout of the possible conformation of **ON17** displaying stacking interaction between two anthraquinone moieties in one benzene ring. Stacked benzene rings in both H_{26} monomers are marked in magenta, while the rest of the two linkers are in cyan. Cytidine base pairs are shown in lime green. Thymidines (**T**) and adenosines (**A**) are shown in orange.

Conclusions

Herein, four isomeric DMT 1,8-, 1,4-, 1,5- and 2,6-bis(3-hydroxypropoxy)anthraquinone phosphoramidites have been incorporated into oligonucleotides and their replacements of the central and the outer **TAA** loops in the 22mer C-rich human telomeric DNA sequence are discussed. Increased thermal stabilities were observed in all possible modifications at the central **TAA** loop of the i-motif structures. The largest stabilization at the thermal melting temperature was shown for position T_{10} upon replacing H_{26} and the increase was found to be 8.2 °C. Molecular models support the increase in T_m due to improved stacking interactions and hydrogen bonding in the i-motif construct. Also, a pair of H_{26} resulted in a considerable increase in the i-motif stability (ΔT_m = 5.0 °C). According to molecular modeling, this could be a result of the increased stacking of the H_{26} pair on each other. The substitution pattern of the linker attached to the anthraquinone moiety is crucial for improving the stability of the i-motifs as demonstrated by H_{18}, H_{14} and H_{15} monomers showing lower thermal stabilities for insertions into the loop regions of i-motifs in contrast to H_{26} which revealed a substantial improvement in the thermal stability. According to circular dichroism (CD) spectral analysis, no changes in the i-motif structure and folding molecularity were observed confirming the compatibility of anthraquinone modified oligonucleotides to adopt the i-motif structure based on hemiprotonated C–C^+ base pairs. Non-nucleoside anthraquinone monomers have for the first time been studied in the context of an i-motif, and hence, could be useful tools to modulate the thermal stability of telomeric i-motif DNA. The new anthraquinone monomers reported here offer a set of artificial building blocks with potential applications in DNA-based therapeutics. More specifically, our data open up for further development of our previously described novel i-motif decoy strategy in cancer therapy.[11] In fact, the reported studies could give a unique opportunity to develop i-motif based technologies since the anthraquinone insertions are compatible with the syntheses of numerous modified oligonucleotides. Furthermore, the obtained findings give insights into the general characteristics of anthraquinones when used to modulate oligonucleotide architectures.

Experimental section

General

Commercially available dC, dA and dT DNA phosphoramidite monomers, the wild type DNA oligonucleotide, solid supports and additional reagents were purchased from Sigma-Aldrich or Glen Research. Acetonitrile and 5-[3,5-bis(trifluoromethyl)

phenyl]-1*H*-tetrazole (required for the hand coupling of anthraquinone phosphoramidites) were dried over activated molecular sieves (3 Å) and their dryness was estimated using a Karl Fischer titrator (<10 ppm). The synthesized oligonucleotides have been purified by ion-exchange chromatography. HPLC grade acetonitrile or methanol was used as the solvent. The composition of the synthesized oligonucleotide (Table S1, ESI†) was verified by MALDI-TOF analysis on a Bruker Daltonics Microflex LT (MALDI-LIFT system) MS instrument in the ES^+ mode with a HPA-matrix (10 mg 3-hydroxypicolinic acid in 50 mM ammoniumcitrate/70% acetonitrile).

Oligonucleotide synthesis and purification

Oligonucleotides were synthesized as described previously from the anthraquinone phosphoramidites corresponding to **H_{18}**, **H_{14}**, **H_{15}** and **H_{26}** monomers with the hand-coupling times extended to 15 minutes for the anthraquinone amidites[37,40] using 5-[3,5-bis(trifluoromethyl)phenyl]-1*H*-tetrazole (0.25 M, in dry acetonitrile) as an activator. Due to their high sensitivity to humidity and light, the DMT-protected phosphoramidites were immediately used on a PerSeptive Biosystems expedite™ 8909 automated DNA/RNA synthesizer in a 0.2 μmol scale on a 500 Å CPG support using the standard phosphoramidite cycle protocol. Stepwise coupling efficiencies, determined by the absorbance of trityl cations at 495 nm on a UV-VIS spectrophotometer, were in the range 83–99% for the synthesized phosphoramidites.

The removal of nucleobase protecting groups and cleavage from the solid support were carried out under standard conditions (1 ml of 32% aqueous ammonia, 12 h at 55 °C). The resulting oligonucleotides **ON8–ON29** and **ON33** were purified by DMTr-ON reversed phase HPLC (RP-HPLC) using a Waters system 600 equipped with a XBridge OBD C18-column (19 × 1000 mm, 5 μm + precolumn: XBridge 10 × 10 mm, 5 μm, temperature column oven: 50 °C). Elution was performed starting with an isocratic hold of buffer A for 2 min followed by a linear gradient to 70% buffer B over 17 min at a flow rate of 5 mL min^{-1} (buffer A: 0.05 M triethylammonium acetate in Milli-Q water, pH 7.4; buffer B: 75% CH_3CN/25% buffer A).

ON1, **ON2–ON7**, and **ON30–ON32** were used without RP-HPLC purification. **ON32** seemed to be pure enough and was initially precipitated without purification, but a purity of less than 80% was observed after precipitation. Therefore, it was purified by anion-exchange HPLC (IE-HPLC) using the DIONEX Ultimate 3000 system equipped with a DNAPac PA100 semipreparative column (13 μm, 250 mm × 9 mm) heated to 60 °C. Elution was performed with an isocratic hold of buffer B (10%), starting from a 2 min hold on 2% buffer A in Milli-Q water (solvent A), followed by a linear gradient to 25% buffer A in 20 min at a flow rate of 1.0 mL min^{-1} (buffer A: 1.0 M sodium perchlorate; buffer B: 0.25 M TrisCl, pH 8.0, solvent A: Milli-Q water). After IE-HPLC purification, the oligonucleotide was desalted using a NAP™-10 column (illustra™, GE Healthcare, prepacked with Sephadex™ G-25 DNA-grade resin, input sample volume up to 1 mL) according to the manufacturer's instructions.

After removing the solvents under a nitrogen flow, oligonucleotides were detrityled by treatment with 100 μL of 80% aqueous solution of acetic acid for 30 min and 100 μL double filtered water, and then an aqueous solution of sodium acetate (3 M, 15 μL) and sodium perchlorate (5 M, 15 μL) was added, followed by cold acetone (1 mL). The resulting suspension was stored at −20 °C for 1 h. After centrifugation (13 000 rpm, 10 min, 4 °C), the supernatant was removed and the pellet further washed with cold acetone (2 × 1 mL), dried for 30 min under a nitrogen flow, and dissolved in MilliQ water (1000 μl). The MALDI-TOF analysis of **ON16** showed that there were subsequent +99.5 (a.m.u) increases over the exact mass of the oligo. This could be compatible with contaminated perchlorate anions. Therefore, **ON16** underwent a desalting process using the NAP™-10 column (illustra™, GE Healthcare, prepacked with Sephadex™ G-25 DNA-grade resin, input sample volume up to 1 mL) according to the manufacturer's instructions.

The purity of the final oligodeoxynucleotides (except for **ON8**, **ON12**, **ON15**, **ON20**, **ON21**, **ON23** and **ON29**, the purity was 100%) was found to be more than 90% when recorded by analytical IE-HPLC traces on a Merck Hitachi La-Chrom system equipped with a DNAPac PA100 analytical column (13 μm, 250 mm × 4 mm) heated to 60 °C. Elution was performed with an isocratic hold of buffer (10%), starting from a 2 min hold on a 2% eluent in Milli-Q water (solvent A), followed by a linear gradient to a 30% eluent in 23 min at a flow rate of 1.1 mL min^{-1} (eluent A: 1.0 M sodium perchlorate; buffer: 0.25 M Tris-Cl, pH 8.0; solvent A: Milli-Q water).

Thermal melting studies of i-motifs

Thermal melting measurements were carried out with solutions of DNA oligomers on a Perkin-Elmer Lambda 35 UV–Vis spectrometer fitted with a PTP-6 peltier temperature programmer using Hellma SUPRASIL synthetic quartz optical cuvettes with a path length of 10.0 mm. Concentrations of purified oligonucleotides were determined by using UV at 260 nm, assuming identical molar absorptivities for unmodified DNA nucleotides (ε_{260}: **dC** = 7.3, **dA** = 13.7, **dT** = 8.4 OD_{260} per μmol). Extinction coefficients were determined for the four isomeric anthraquinone moieties (ε_{260} = 9.6, 8.36, 24.68, and 11.15 OD_{260} per μmol for **H_{14}**, **H_{18}**, **H_{15}** and **H_{26}** respectively) after measuring the absorbance averages of three measurements for each linker. The synthesized oligonucleotides (4 μM) were mixed with potassium buffer (100 mM KCl, 20 mM K_2HPO_4 and 1 mM K_2EDTA at pH 5.5) to furnish i-motif forming oligonucleotides. The samples were heated to 80 °C (15 min) after transferring them into the cuvettes, followed by cooling to the starting temperature of the experiment 25 °C, and then they were kept at this temperature for 120 min. The thermal melting temperatures (T_m, °C) were determined as the maximum of the first derivative plots of the smoothed melting curves obtained by UV absorbance at 295 nm against increasing temperature from 25 °C to 65 °C (gradient: 0.5 °C min^{-1}) programmed by a Peltier temperature controller. All melting temperatures are within the uncertainty of ±0.5 °C as determined by repetitive experiments and the T_m values were calcu-

lated using UV-WinLab software, taking an average of the two melting curves.

Circular dichroism spectra

CD spectroscopy has been performed on a Jasco J-600A spectropolarimeter using 1 mL quartz cuvettes with 5 mm path length. Oligonucleotides (4 μM) were dissolved in a buffer containing 100 mM KCl, 20 mM K_2HPO_4, and 1 mM K_2EDTA at pH 5.5. All samples were heated for 2 minutes at 80 °C and slowly cooled to room temperature before data collection. The measurements were performed at 20 °C in the 200–400 nm wavelength range with a continuous scanning mode, 50 nm min^{-1} as scanning speed, 4 s as response time, 2.0 nm asbandwidth and accumulation 5 times. The buffer spectrum was subtracted from the sample spectra. The spectra were smoothened in Microcal Origin 6.0 using a Savitzky–Golay filter.

Molecular modelling

Molecular modelling was carried out using Maestro v9.2 from Schrödinger. All calculations were conducted using the AMBER* force field[49] and the GB/SA water model[50] as implemented by MacroModel. Extended cut-offs were used for non-bonded interactions (van der Waals: 8 Å and electrostatics: 20 Å). The molecular dynamic simulations were performed with stochastic dynamics, a SHAKE algorithm to constrain bonds to H-atoms, at a time step of 1.5 fs, and a simulation temperature of 300 K. Simulation for 0.5 ns with an equilibration time of 150 ps generated 250 individual structures, which were minimized using the PRCG method[51] with maximum iterations of 5000 and a convergence threshold of 0.05 kJ mol^{-1}. The global minimum was used for analysis. The starting structures were generated using the Protein Data Bank (PDB) code (1El2 accession number), followed by the incorporation of the anthraquinone monomer $\mathbf{H_{26}}$. The resulting structures were further processed in PyMOL (v1.7.4.5, 2010. http://pymol.org) and in VMD (v1.9.3a6, 2015. http://www.ks.uiuc.edu) molecular graphics systems.

Acknowledgements

We greatly appreciate the financial support from the Cultural Affairs & Missions Sector, Egyptian Ministry of Higher Education for funding the Ph.D. Scholarship holder Alaa S. Gouda. Tina Grubbe Hansen is thanked for the excellent technical assistance in the purification of oligonucleotides.

References

1 H. Tateishi-Karimata, M. Nakano, S. Pramanik, S. Tanaka and N. Sugimoto, *Chem. Commun.*, 2015, **51**, 6909–6912.
2 K. Gehring, J. L. Leroy and M. A. Guéron, *Nature*, 1993, **363**, 561–565.
3 A. T. Phan, M. Guéron and J.-L. Leroy, *J. Mol. Biol.*, 2000, **299**, 123–144.
4 R. D. Wells, D. A. Collier, J. C. Hanvey, M. Shimizu and F. Wohlrab, *FASEB J.*, 1988, **2**, 2939–2949.
5 A. Pasternak and J. Wengel, *Bioorg. Med. Chem. Lett.*, 2011, **21**, 752–755.
6 J.-F. Cornuel, A. Moraillon and M. Guéron, *Biochimie*, 2002, **84**, 279–289.
7 M. Kaushik, M. Prasad, S. Kaushik, A. Singh and S. Kukreti, *Biopolymers*, 2009, **93**, 150–160.
8 Z. Yu, V. Gaerig, Y. Cui, H. Kang, V. Gokhale, Y. Zhao, L. H. Hurley and H. Mao, *J. Am. Chem. Soc.*, 2012, **134**, 5157–5164.
9 S. Kendrick, H.-J. Kang, M. P. Alam, M. M. Madathil, P. Agrawal, V. Gokhale, D. Yang, S. M. Hecht and L. H. Hurley, *J. Am. Chem. Soc.*, 2014, **136**, 4161–4171.
10 D. Sun and L. H. Hurley, *J. Med. Chem.*, 2009, **52**, 2863–2874.
11 G. Miglietta, S. Cogoi, E. B. Pedersen and L. Xodo, *Sci. Rep.*, 2015, **5**, 18097.
12 M. Guéron and J.-L. Leroy, *Curr. Opin. Struct. Biol.*, 2000, **10**, 326–331.
13 N. Kumar, J. T. Nielsen, S. Maiti and M. Petersen, *Angew. Chem., Int. Ed.*, 2007, **46**, 9220–9222.
14 J. L. Leroy, K. Gehring, A. Kettani and M. Guéron, *Biochemistry*, 1993, **32**, 6019–6031.
15 A. L. Lieblein, M. Kramer, A. Dreuw, B. Furtig and H. Schwalbe, *Angew. Chem., Int. Ed.*, 2012, **51**, 4067–4070, (*Angew. Chem.*, 2012, **124**, 4143–4146).
16 P. Alberti, A. Bourdoncle, B. Sacca, L. Lacroix and J. L. Mergny, *Org. Biomol. Chem.*, 2006, **4**, 3383–3391.
17 J. Cui, P. Waltman, V. H. Le and E. A. Lewis, *Molecules*, 2013, **18**, 12751–12767.
18 D. Collin and K. Gehring, *J. Am. Chem. Soc.*, 1998, **120**, 4069–4072.
19 M. Garavís, N. Escaja, V. Gabelica, A. Villasante and C. González, *Chem. – Eur. J.*, 2015, **21**, 9816–9824.
20 H. A. Day, E. P. Wright, C. J. MacDonald, A. J. Gates and Z. A. E. Waller, *Chem. Commun.*, 2015, **51**, 14099–14102.
21 F. Seela and S. Budow, *Helv. Chim. Acta*, 2006, **89**, 1978–1985.
22 S. Modi, M. G. Swetha, D. Goswami, G. D. Gupta, S. Mayor and Y. Krishnan, *Nat. Nanotechnol.*, 2009, **4**, 325–330.
23 Y. Peng, X. Wang, Y. Xiao, L. Feng, C. Zhao, J. Ren and X. Qu, *J. Am. Chem. Soc.*, 2009, **131**, 13813–13818.
24 (*a*) Y. Dong, Z. Yang and D. Liu, *Acc. Chem. Res.*, 2014, **47**, 1853–1860; (*b*) H. A. Day, P. Pavlou and Z. A. E. Waller, *Bioorg. Med. Chem.*, 2014, **22**, 4407–4418.
25 T. Liedl, M. Olapinski and F. C. Simmel, *Angew. Chem., Int. Ed.*, 2006, **45**, 5007–5010.
26 G. Cimino-Reale, E. Pascale, E. Alvino, G. Starace and E. D'Ambrosio, *J. Biol. Chem.*, 2003, **278**, 2136–2140.
27 S. Neidle, R. J. Harrison, A. P. Reszka and M. A. Read, *Pharmacol. Ther.*, 2000, **85**, 133–139.
28 M. A. Blasco, *Eur. J. Cell Biol.*, 2003, **82**, 441–446.
29 S. Benabou, A. Aviño, R. Eritja, C. Gonzalez and R. Gargallo, *RSC Adv.*, 2014, **4**, 26956–26980.

30 S. Kendrick, Y. Akiyama, S. M. Hecht and L. H. Hurley, *J. Am. Chem. Soc.*, 2009, **131**, 17667–17676.
31 N. Kumar, M. Petersen and S. Maiti, *Chem. Commun.*, 2009, **12**, 1532–1534.
32 P. Perlíková, K. K. Karlsen, E. B. Pedersen and J. Wengel, *ChemBioChem*, 2014, **15**, 146–156.
33 A. A. El-Sayed, E. B. Pedersen and N. A. Khaireldin, *Nucleosides, Nucleotides Nucleic Acids*, 2012, **31**, 872–879.
34 (*a*) N. Bouquin, V. L. Malinovskii and R. Häner, *Eur. J. Org. Chem.*, 2008, 2213–2219; (*b*) C. Percivalle, C. Sissi, M. L. Greco, C. Musetti, A. Mariani, A. Artese, G. Costa, M. L. Perrore, S. Alcaro and M. Freccero, *Org. Biomol. Chem.*, 2014, **12**, 3744–3754; (*c*) G. Zagotto, A. Ricci, E. Vasquez, A. Sandoli, S. Benedetti, M. Palumbo and C. Sissi, *Bioconjugate Chem.*, 2011, **22**, 2126–2135.
35 G. Miglietta, A. S. Gouda, S. Cogoi, E. B. Pedersen and L. E. Xodo, *ACS Med. Chem. Lett.*, 2015, **6**, 1179–1183.
36 A. Membrino, S. Cogoi, E. B. Pedersen and L. E. Xodo, *PLoS One*, 2011, **6**, e24421.
37 A. S. Gouda, M. S. Amine and E. B. Pedersen, *Helv. Chim. Acta*, 2016, **99**, 116–124.
38 E. P. Wright, H. A. Day, A. M. Ibrahim, J. Kumar, L. J. E. Boswell, C. Huguin, C. E. M. Stevenson, K. Pors and Z. A. E. Waller, *Sci. Rep.*, 2016, **6**, 39456.
39 J. Choi, A. Tanaka, D. Won Cho, M. Fujitsuka and T. Majima, *Angew. Chem., Int. Ed.*, 2013, **52**, 12937–12941.
40 A. S. Gouda, M. S. Amine and E. B. Pedersen, *Eur. J. Org. Chem.*, 2017, 3092–3100.
41 P. Nielsen, L. H. Dreiøe and J. Wengel, *Bioorg. Med. Chem. Lett.*, 1995, **3**, 19–28.
42 G. Manzini, N. Yathindra and L. E. Xodo, *Nucleic Acids Res.*, 1994, **22**, 4634–4640.
43 Y. Krishnan-Ghosh, E. Stephens and S. Balasubramanian, *Chem. Commun.*, 2005, **42**, 5278–5280.
44 N. K. Sharma and K. N. Ganesh, *Chem. Commun.*, 2005, **34**, 4330–4332.
45 S. Modi, A. H. Wani and Y. Krishnan, *Nucleic Acids Res.*, 2006, **34**, 4354–4363.
46 J. A. Brazier, J. Fisher and R. Cosstick, *Angew. Chem., Int. Ed.*, 2006, **45**, 114–117.
47 R. Cosstick, J. Buckingham, J. Brazier and J. Fisher, *Nucleosides, Nucleotides Nucleic Acids*, 2007, **26**, 555–558.
48 C. P. Fenna, V. J. Wilkinson, J. R. P. Arnold, R. Cosstick and J. Fisher, *Chem. Commun.*, 2008, **30**, 3567–3569.
49 S. J. Weiner, P. A. Kollman, D. A. Case, U. C. Singh, C. Ghio, G. Alagona, S. Profeta and P. Weiner, *J. Am. Chem. Soc.*, 1984, **106**, 765–784; S. J. Weiner, P. A. Kollman, D. T. Nyguyen and D. A. Case, *J. Comput. Chem.*, 1986, **7**, 230–252.
50 W. C. Still, A. Tempczyk, R. C. Hawlay and T. Hendrickson, *J. Am. Chem. Soc.*, 1990, **112**, 6127–6129.
51 E. Polak and G. Ribière, *Rev. Francaise Informat Recherche Operationelle*, 1969, **16**, 35–43.